J. Fluid Mech. (1975), *vol.* 69, *part* 1, *pp.* 109–128
Printed in Great Britain

The development of weak waves in the steady two-dimensional flow of a gas with vibrational relaxation past a thin wedge

By R. P. HORNBY† AND N. H. JOHANNESEN
Department of the Mechanics of Fluids, University of Manchester, England

(Received 16 September 1974)

The method of characteristics is used to calculate the supersonic flow past a wedge of small angle with non-equilibrium effects. The wave decay and development distances are presented in a concise similarity form which permits accurate extrapolation to very weak waves. The numerical solutions are compared with shock-tube flows of CO_2 and N_2O.

1. Introduction

The steady one-dimensional flow of a relaxing gas through a normal shock wave has been extensively treated in the literature, and it is well known that it is possible to construct oblique shock waves from one-dimensional solutions by the superposition of a velocity component parallel to the wave. In particular, it is found that fully dispersed normal shock waves, which occur when the speed of the approaching flow lies between the equilibrium and frozen sound speeds, lead to fully dispersed oblique shock waves when the deflexion through the wave is sufficiently small.

In the flow past bodies with discontinuous changes in surface slope the shock waves and expansion waves are frozen close to the surface, and the shock waves conform to the one-dimensional analogy only far from the body; indeed, for complicated body shapes it is difficult to assess whether the shock waves can ever be truly represented by the one-dimensional equations.

In this paper we consider the simplest possible case of the two-dimensional flow past a thin wedge and study the development of the wave from the wedge tip to a large distance from the wedge. The analogous one-dimensional unsteady problem of the development of the wave from a piston started impulsively from rest with a small velocity is investigated in the adjacent paper by Dain & Hodgson (1975).

The weak-wave analyses for these two flows are very similar (see Blythe 1969). A number of papers have presented approximate treatments of these flows but it is difficult to obtain precise numerical results which accurately account for the essentially nonlinear effects which cause the gradual change from the initially frozen shock wave at the origin of the disturbance to the fully developed wave at

---

† Present address: Department of Mechanical Engineering, University of Liverpool.

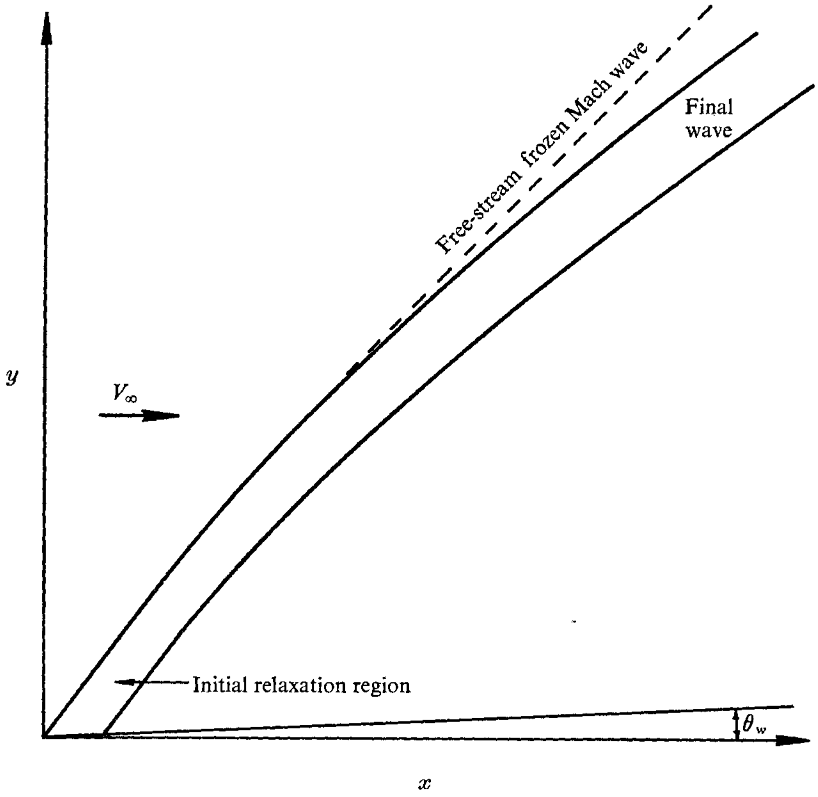

FIGURE 1. Schematic diagram of flow field with fully dispersed wave at infinity.

infinity, in which convective and diffusive effects balance to give a stable wave form (see Lighthill 1956). This is perhaps not surprising when it is appreciated that, although the flow may be a small perturbation of the initially uniform conditions, the non-equilibrium effects are not a small perturbation of the ideal-gas conical flows with a straight constant-strength shock wave.

The flow considered is shown schematically in figure 1, where we have chosen Cartesian co-ordinates with the x axis in the direction of the free stream, whose velocity is V_∞. Distances and changes in angles have been distorted to indicate clearly the significant features of the flow. The shock wave at the wedge tip will instantaneously deflect the flow through the wedge angle θ_w and is therefore a frozen shock inclined at the appropriate wave angle ϕ_0. We shall refer to solutions which retain all terms in the governing inviscid equations as exact. The flow at the wedge tip is therefore known exactly and the flow near the tip is frozen to the first approximation. At infinity, defined as where both $x \to \infty$ and $y \to \infty$, we expect a shock wave of constant width and direction with equilibrium conditions both upstream and downstream. Since all streamlines far downstream of the shock must be parallel to the wedge surface we can conclude that the shock wave at infinity resides at a wave angle corresponding to an equilibrium flow deflexion θ_w. The wave structure, but not the location of the wave, can be found exactly by integrating the conservation, rate and state equations normally through the wave interior.

The frozen shock wave at the tip decays with increasing distance from the wedge surface, and the equilibrium shock angle is less than the corresponding frozen shock angle. In the limit $\theta_w \rightarrow 0$ the two angles degenerate into the equilibrium and frozen Mach angles, respectively. The normal frozen Mach number at infinity may be greater than, equal to or smaller than one. The latter two cases lead to fully dispersed waves, while in the first case the wave is partly dispersed and consists of a frozen discontinuity followed by a relaxation region.

To determine the flow we must determine the decay of the frozen shock and the history of the development of the wave towards its ultimate 'one-dimensional' form. Far downstream we have equilibrium conditions, and the pressure and flow angles are uniform. Other properties, however, change from streamline to streamline because of the different initial histories of particles on different streamlines. We shall concentrate on flows with fully dispersed or weak, partly dispersed waves at infinity, i.e. on flows with small θ_w (in the appropriate sense), but the general calculation methods are equally applicable to flows with strong shock waves.

The weak-wave flows are particularly interesting because the differences between non-equilibrium and frozen (or ideal-gas) flows are very large. Also, the conventional relaxation length no longer serves as a characteristic length scale. It was pointed out by Hodgson & Johannesen (1971) that the thickness of fully dispersed waves may be orders of magnitude greater than the relaxation length. The development length scale along the wave is of course even larger.

2. Calculation procedure and a typical example

Because of the inadequacy of the analytical methods the flows must be calculated numerically, and of the available methods we have chosen the method of characteristics, which, although lengthy, is probably the most accurate and also has the advantage of being closely related to the actual physical features of the flow.

We introduce non-dimensional variables based on free-stream conditions. A prime indicates a dimensional quantity and in what follows all unprimed variables are non-dimensional.

$$p' = p'_\infty p, \quad \rho' = \rho'_\infty \rho, \quad T' = T'_\infty T, \tag{1)-(3}$$

$$(V', u', v') = (R'T'_\infty)^{\frac{1}{2}} (V, u, v), \tag{4}$$

$$(c'_p, c'_{\mathrm{vib}}, s') = R'(c_p, c_{\mathrm{vib}}, s), \tag{5}$$

$$\sigma' = R'T'_\infty \sigma, \quad \Phi' = \Phi'_\infty \Phi \tag{6), (7}$$

and

$$(x', y', \ldots) = (R'T'_\infty)^{\frac{1}{2}}/(\rho'_\infty \Phi'_\infty)\,(x, y, \ldots). \tag{8}$$

p, ρ and T are the pressure, density and translational temperature, u and v are the velocity components, R' the gas constant, s the real-gas entropy, σ the vibrational energy, c_p and c_{vib} the frozen and vibrational specific heats, and Φ is the relaxation frequency defined by the simple relaxation equation

$$D\sigma/Dt = \rho\Phi(\bar{\sigma}-\sigma), \tag{9}$$

where the bar indicates the equilibrium value of σ, which is a function of T only.

The flow equations become in characteristic form (e.g. see Der (1963) and change the notation slightly)

$$dy/dx = \tan(\theta+\mu), \tag{10}$$

$$\frac{dp}{\rho V^2 \tan\mu}+d\theta = -\frac{(\gamma-1)\rho\Phi(\bar{\sigma}-\sigma)}{V^3\sin\mu\sin(\theta+\mu)}dy \tag{11}$$

on the left-hand characteristics,

$$dy/dx = \tan(\theta-\mu), \tag{12}$$

$$\frac{dp}{\rho V^2 \tan\mu}-d\theta = -\frac{(\gamma-1)\rho\Phi(\bar{\sigma}-\sigma)}{V^3\sin\mu\sin(\theta-\mu)}dy \tag{13}$$

on the right-hand characteristics, and

$$\frac{dy}{dx} = \tan\theta, \quad dp = -\rho V\,dV, \quad d\sigma = \frac{\rho\Phi(\bar{\sigma}-\sigma)}{V\sin\theta}dy \qquad (14)\text{–}(16)$$

on the streamlines. Here μ is the frozen Mach angle and γ the frozen specific-heat ratio. In addition the equations of energy and state are valid everywhere in the flow:

$$c_pT+\sigma+\tfrac{1}{2}V^2 = \text{constant}, \tag{17}$$

$$p = \rho T. \tag{18}$$

The last equation is in fact the only equation which differs from its dimensional form, by the absence of the gas constant R'.

Viscosity and heat conduction have been neglected throughout. This restriction is no more severe than in ordinary ideal-gas compressible flow theory.

The boundary conditions for the above set of equations are $\theta = \theta_w$ on the wedge surface together with the conditions on the frozen shock wave, i.e. conditions immediately downstream of the shock must satisfy the oblique frozen shock wave relations. It should be noted that the location of the shock wave and its local angle are not known *a priori*.

To proceed with a numerical calculation we require the functional relationships $\bar{\sigma}(T)$ and $\Phi(T)$. However, if we confine ourselves to weak-wave flows then both functions vary only slightly in the small intervals of T encountered and the general features of the flows will not be affected by putting

$$\Phi = 1, \quad d\bar{\sigma}/dT = c_{\text{vib}} = \text{constant}, \qquad (19), (20)$$

so that

$$\bar{\sigma} = \bar{\sigma}_\infty + c_{\text{vib}}(T-1). \tag{21}$$

In the cases considered the errors introduced by these simplifications will not exceed 10%. It is straightforward to make more accurate calculations by incorporating the proper functional relations for $\bar{\sigma}$ and Φ in the computer program.

A network based on the left-hand and right-hand characteristics and using interpolation along the streamlines at each network point was chosen. Because of the very gradual changes in the far field it was not obvious at the outset that the conventional step-by-step method would work when the neighbouring characteristics become nearly parallel to the shock wave. Certainly, the usual choice of equal step sizes along the wedge surface or the shock wave would have led to a prohibitively large number of steps in the far field. We therefore chose a 'thermodynamic' step size; more precisely, steps along the wedge surface were chosen which all corresponded to roughly equal changes in σ. This led to steps which corresponded to similar changes in the thermodynamic variables, although the geometric step size varied greatly. With this network the calculations proceeded smoothly without difficulties or instabilities and resulted in a surprising accuracy. The usual check on the accuracy by varying the step size was supplemented by conservation checks. The integrated energy equation is incorporated in the calculation procedure and is therefore automatically satisfied. The momentum and continuity equations were integrated along left-hand characteristics and found to be satisfied in general with an accuracy of the order of 1 %.

A special procedure was needed for the flows with fully dispersed waves at infinity. Here the shock wave decays to zero strength before the calculation is completed. This manifested itself by an overshoot to negative shock strengths but was easily dealt with by interpolating to zero strength and then replacing the shock wave by a frozen Mach wave in the remaining steps at the front of the flow field.

A very important additional check is possible with the flows considered here because we know the exact wave profiles at infinity if not their locations. Direct integration of the conservation equations in a direction normal to the wave at infinity gives the profiles of all variables. This is true whether the wave at infinity is fully dispersed or partly dispersed. To avoid difficulties at the ends of a fully dispersed wave profile, where the gradients are very small, it is best to integrate in both directions from the point of inflexion. An outline of the method is given by Hodgson & Johannesen (1971).

The solution can be projected along any curve in the x, y plane. For ease of comparison with the computer output we in general used projections along the characteristics.

To decide which flows to calculate we must first discuss which parameters control the flow. The free-stream pressure and relaxation frequency per unit density do not affect the physical nature of the flow but simply scale the coordinates and have already been incorporated in the non-dimensionalization θ_w. and M_∞, the frozen free-stream Mach number, are obvious parameters and an examination of the non-dimensional governing equations reveals that apart from γ, which we shall keep constant, the only other unspecified parameter is c_{vib}. We have already made the assumption of a constant but different specific heat for each flow. For any real gas the free-stream temperature is defined implicitly by c_{vib}. For example, if we calculate a set of flows with $c_{\mathrm{vib}} = 1{\cdot}00$ then these calculations are valid for all those flows with a free-stream temperature for which $c_{\mathrm{vib}} = 1{\cdot}00$.

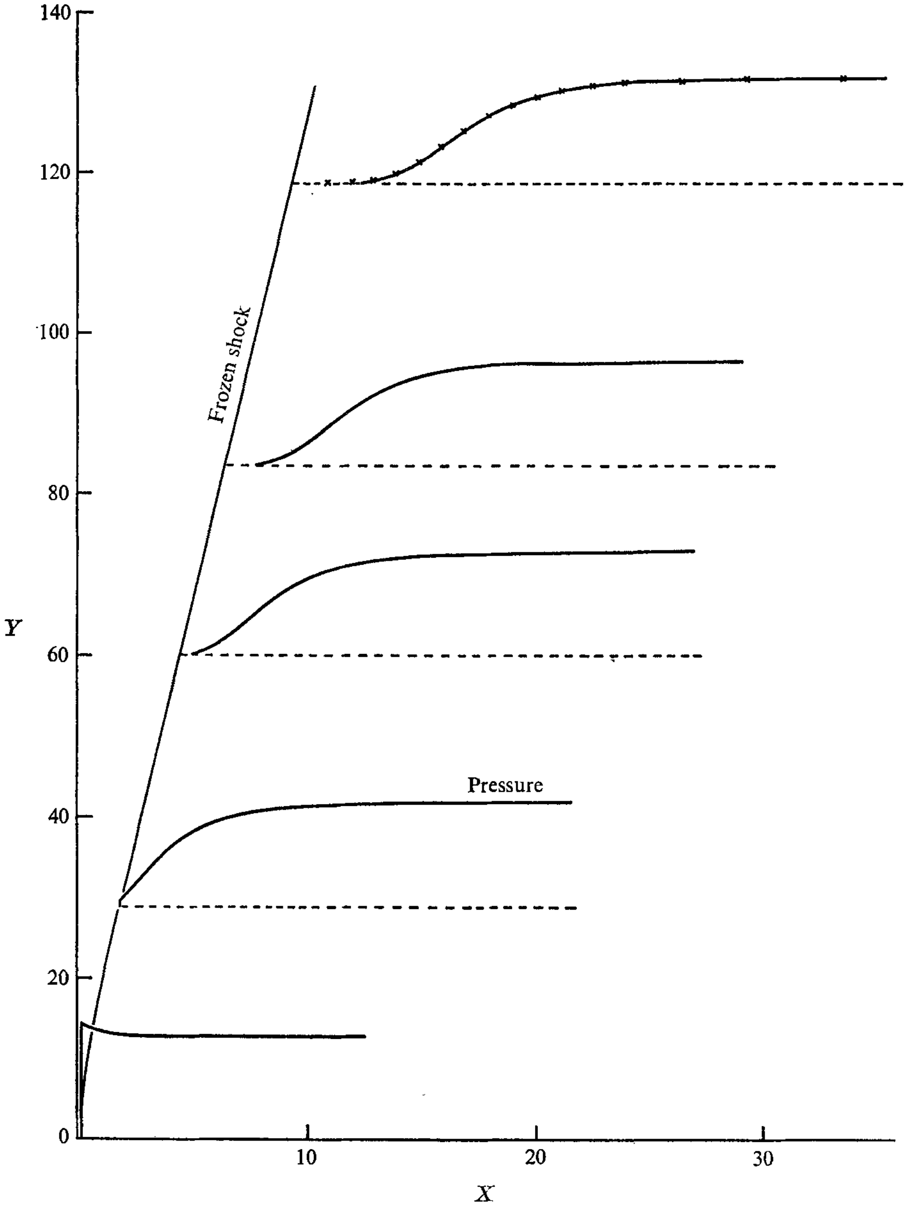

FIGURE 2. Pressure profiles along the wave. ×, exact solution at infinity, $\theta_w = 2{\cdot}00°$, $M_\infty = 1{\cdot}49$, $c_{\text{vib}} = 2{\cdot}12$.

We chose discrete values $M_\infty = 1{\cdot}4$, $2{\cdot}6$ and $3{\cdot}8$ and $c_{\text{vib}} = 0{\cdot}5$, 1, 2 and 3 and calculated 48 flows, covering a range of θ_w from $0{\cdot}2°$ to $4{\cdot}4°$ and including both fully dispersed and weak, partly dispersed waves at infinity.

We shall illustrate the calculation procedure by looking in detail at the calculation of one particular flow, that with $\theta_w = 2{\cdot}00°$, $M_\infty = 1{\cdot}49$ and $c_{\text{vib}} = 2{\cdot}12$. The reason for this particular choice of parameters is that these values correspond

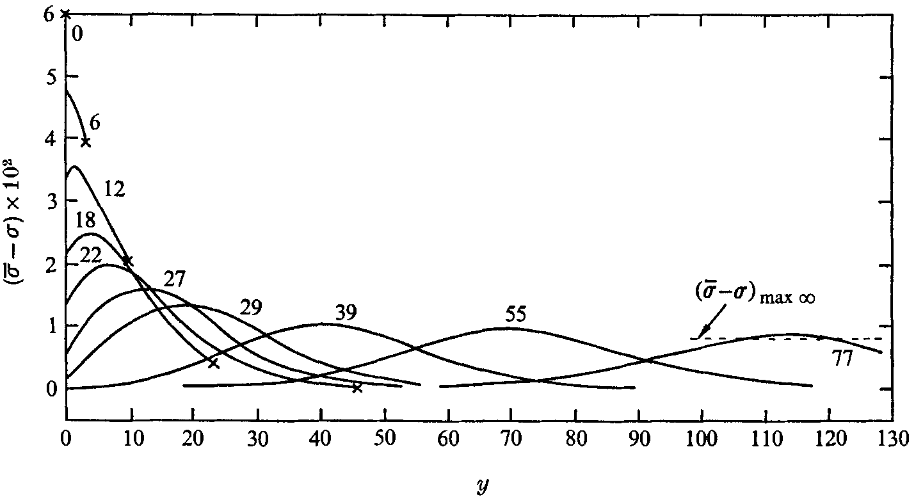

FIGURE 3. Variation of the departure from local equilibrium along successive left-hand characteristics.

to a realizable shock-tube flow of CO_2 at a free-stream temperature of 600 °K. For this particular calculation we used 50 steps along the wedge surface, changing to constant step size after 90 % of the change in vibrational energy had taken place. This final constant step size was about ten times the initial step size. A general picture of the wave development is shown in figure 2, which clearly demonstrates the gradual change from a frozen shock at the tip to a fully dispersed wave at large distances. Also shown is the exact solution at infinity superimposed on the most distant wave profile obtained by the method of characteristics. The agreement is remarkable.

Because the physical (x, y) co-ordinate system involves distances that are both very large and very small in each co-ordinate on the same characteristic (or on the shock wave) we found it more convenient to plot the results in a distorted co-ordinate system defined by

$$X = x - y/\tan\phi_0, \quad Y = y,$$

where ϕ_0 is the initial shock angle.

Figure 3 shows the departure from equilibrium of the vibrational energy $\bar{\sigma}-\sigma$, plotted along the left-hand characteristics emanating from the wedge surface and meeting the frozen shock wave at the point indicated by a cross. Only selected characteristics are shown and are indicated by their numbers. This is a very effective way of showing, in a qualitative manner, all the decay processes in the flow. The development of the equilibrium core, where $\bar{\sigma}=\sigma$, can be traced simply, and the decay of $\bar{\sigma}-\sigma$ on the wedge surface can be seen from the variations near $y = 0$. The maximum value of the departure from equilibrium is always embedded in the relaxation region, so that the path of the maxima represents the wave trajectory. The approach of the maximum to its ultimate value $(\bar{\sigma}-\sigma)_{\max\infty}$ determines the rate at which the wave develops. The decay of the frozen shock is also adequately expressed by following the variations where the left-hand characteristics terminate. Notice how the frozen shock reached zero strength before the maximum value of the departure from equilibrium had reached its asymptotic value at infinity. This was true for all the computed flows which were fully dispersed at infinity and was far more apparent as the wave strength was decreased. The non-uniformities in the flow variables far downstream near the wedge are not exhibited on this figure because $\bar{\sigma}-\sigma$ is zero in this region.

The decay and development processes are best analysed quantitatively by first normalizing quantities and then plotting on a logarithmic scale. We shall represent all decay and development processes by using the departure from equilibrium $\Gamma = \bar{\sigma}-\sigma$, and shall normalize this quantity for the specific process under discussion in the following ways.

The frozen shock decay is represented by plotting $(\Gamma_\alpha - \Gamma_{\alpha\infty})/(\Gamma_0 - \Gamma_{\alpha\infty})$ against y. Here Γ_α is the departure from equilibrium at the frozen shock, Γ_0 its value at the wedge tip and $\Gamma_{\alpha\infty}$ its value at infinity. If the wave is fully dispersed at infinity, $\Gamma_{\alpha\infty} = 0$ and the expression to be plotted reduces to Γ_α/Γ_0.

The shock wave development is illustrated by plotting

$$(\Gamma_{\max} - \Gamma_{\max\,\infty})/(\Gamma_0 - \Gamma_{\max\,\infty})$$

against y. Here $\Gamma_{\max}$ is the maximum value of Γ along a right-hand characteristic and $\Gamma_{\max\infty}$ is the corresponding quantity for the fully developed wave at infinity. Since initially the maximum of Γ is located at the frozen shock, this expression varies between 1 and 0.

The approach towards the equilibrium state on the wedge surface, and hence the appropriate relaxation distance, was investigated by plotting Γ_w/Γ_0 against x, where Γ_w is the value on the wedge surface.

For each decay and development process in this numerical example, the accuracy of the calculation made with steps corresponding to $\frac{1}{50}$ of the total σ variation on the surface was checked by using steps corresponding to $\frac{1}{10}$ and $\frac{1}{250}$ of the σ variation.

By plotting all the results in the above manner we shall be able to define precisely what we mean by development and decay distances. When the three processes were investigated in the region close to the wedge tip they were found to be adequately described by the initial gradients, which are known exactly and are derived in the appendix. Indeed, the whole relaxation process on the wedge could be described by the initial gradient, giving a straight line on a logarithmic plot. The results for the initial behaviour of the shock wave and for the relaxation process on the wedge are therefore not given here. This result for the initial and wedge processes was found to be general and to hold with a high degree of accuracy for all the computed flows.

Figure 4 shows a logarithmic plot of Γ_α/Γ_0 against y for the decay of the frozen shock (in this example the wave was fully dispersed at infinity). This shows that the outer decay of the frozen shock can be adequately represented by the function

$$\Gamma_\alpha/\Gamma_0 = A \exp(-y/y_\alpha), \tag{22}$$

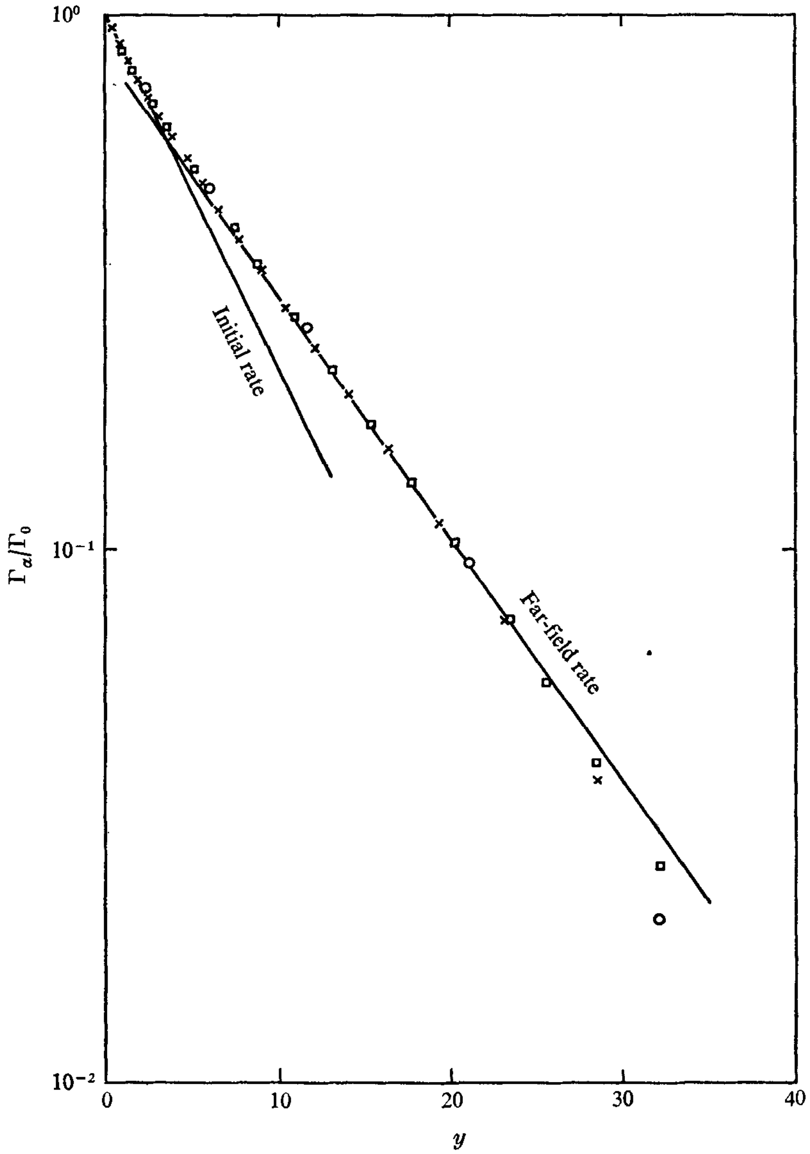

FIGURE 4. Decay of frozen shock. ○, $\frac{1}{10}$ steps; ×, $\frac{1}{50}$ steps; □, $\frac{1}{250}$ steps.

where A represents the value of Γ_α/Γ_0 at $y = 0$ obtained by extending the far-field line on figure 4 to the intersection with $y = 0$, and y_α is a decay distance. Also shown on figure 4 is the line representing the initial gradient given in equation (A 9) in the appendix.

A logarithmic plot of $(\Gamma_{\max} - \Gamma_{\max\,\infty})/(\Gamma_0 - \Gamma_{\max\,\infty})$ is shown in figure 5. Again there are roughly two characteristic rates of development, the first represented by the initial gradient and the other represented by the line

$$(\Gamma_{\max} - \Gamma_{\max\,\infty})/(\Gamma_0 - \Gamma_{\max\,\infty}) = B \exp(-y/y_\beta), \qquad (23)$$

where B is the value at $y = 0$ and y_β is a development distance.

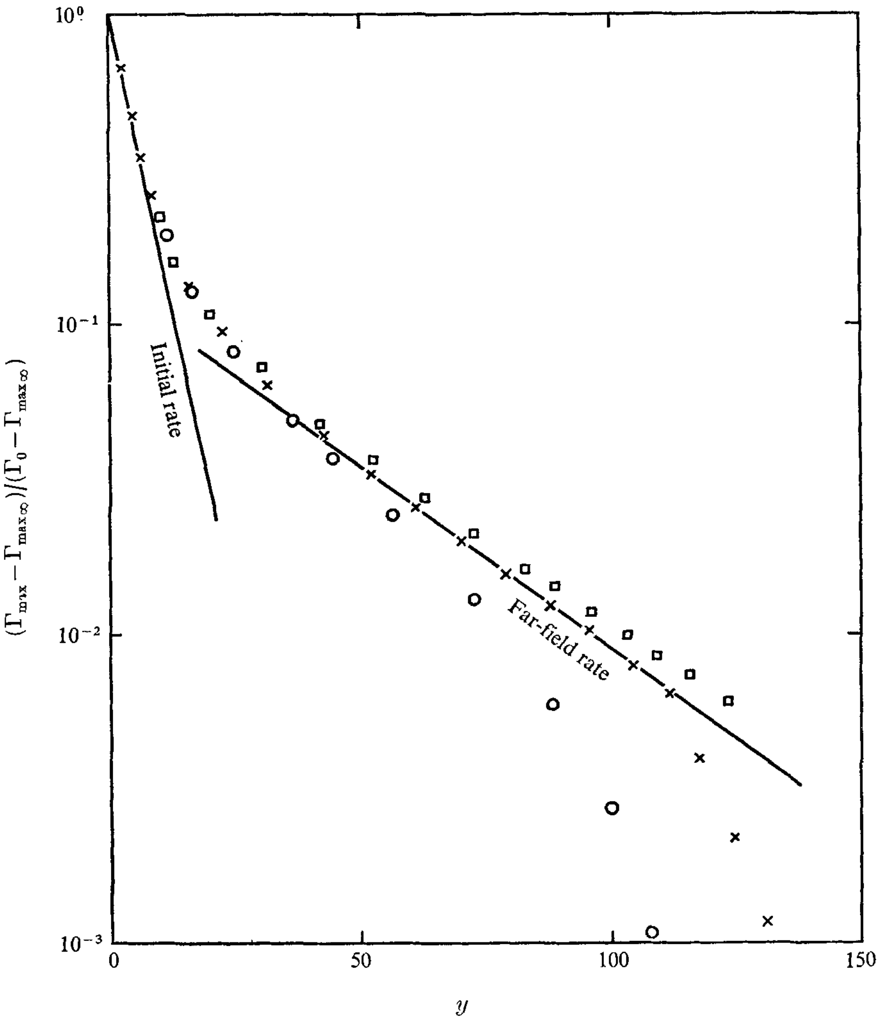

FIGURE 5. Shock wave development. ○, $\frac{1}{10}$ steps; ×, $\frac{1}{50}$ steps; □, $\frac{1}{250}$ steps.

In both figures 4 and 5 points with $\frac{1}{10}$, $\frac{1}{50}$ and $\frac{1}{250}$ step size are indicated. It was concluded that the $\frac{1}{50}$ step size was adequate and for consistency this step size was used in all computations. It should be noted that, not surprisingly, the calculation of the far-field development is less accurate than the calculation of the far-field shock decay. Because of the logarithmic way of plotting, the inaccuracy of the points for large y is of course greatly exaggerated. The percentage scatter is quite small.

Graphs of this type were plotted for all the calculated flows and used for the subsequent analysis. The far-field lines were drawn by hand. This was deemed to be as accurate as any more sophisticated curve-fitting procedure, which would lead to results depending strongly on the precise choice of points to be included.

3. Similarity representation of far-field decay and development processes

All the flows calculated were treated in the same manner as the numerical example in § 2. As already mentioned, the initial behaviour of any flow close to the wedge tip and on the wedge surface was adequately described by the exact initial gradients given in the appendix. The far-field behaviour is characterized by the quantities A and y_α for the frozen shock wave decay and B and y_β for the shock wave development. So far we would expect these quantities to be functions of M_∞, θ_w and c_{vib}. However, when plotting the results in various ways as functions of these parameters and bearing in mind that M_∞ and θ_w can be combined, in so far as shock wave structure at infinity is concerned, into a single variable $M_{n\infty}$, the frozen Mach number normal to the wave at infinity, it was found that what matters for any one flow is the strength of the wave at infinity compared with the strength of the fully dispersed wave of maximum strength at infinity for the same values of M_∞ and c_{vib}.

This led to plotting the quantities against a normalized wedge angle θ_w/θ_w^*, where θ_w^* is the wedge angle which for the particular values of M_∞ and c_{vib} leads to a maximum-strength fully dispersed wave at infinity. In other words, θ_w^* corresponds to the case where the equilibrium wave at infinity lies in the direction of the frozen free-stream Mach lines.

Plots of A and B against θ_w/θ_w^* immediately led to a collapse of all the calculated values, but for y_α and y_β a further normalization was necessary. It was found that a suitable normalization factor was $y_{\alpha l}^{-1}$, where $y_{\alpha l}$ is the well-known linearized-theory frozen-shock decay distance. $y_{\alpha l}$ is usually derived from linearized theory, but a simple derivation from the initial gradients is given in the appendix, equation (A 13). Using $y_{\alpha l}^{-1}$ as a normalizing factor led to the collapse of all calculated values of y_α and y_β onto two single curves when plotted against θ_w/θ_w^*. This shows that although $y_{\alpha l}$ is quite unable to describe the decay of waves of finite strength it does contain the correct functional dependence on M_∞ and c_{vib}.

The resulting curves for y_α, A, y_β and B are given in figures 6 (*a*), (*b*), (*c*) and (*d*). It is felt that the scatter is within the computational and curve-fitting accuracy and that these graphs can therefore be used as universal curves for the prediction of wave decay and development.

It is shown by Dain & Hodgson (1975) that the corresponding analysis of flows generated by an impulsively started piston leads to four universal curves for the far-field which within the computational accuracy are identical to figures 6 (*a*)–(*d*). In particular, if the results of the two papers are combined it is found that for engineering purposes the points in figures 6 (*c*) and (*d*) corresponding to $\theta_w/\theta_w^* < 1$ may be represented by the straight lines

$$y_\beta/y_{\alpha l} = 2{\cdot}0(\theta_w/\theta_w^*)^{-1{\cdot}6} \tag{24}$$

and

$$B = 0{\cdot}27(\theta_w/\theta_w^*). \tag{25}$$

There is no justification for attempting more accurate curve fits, partly because of the numerical errors, but also because relaxation frequencies are never known with a very high accuracy.

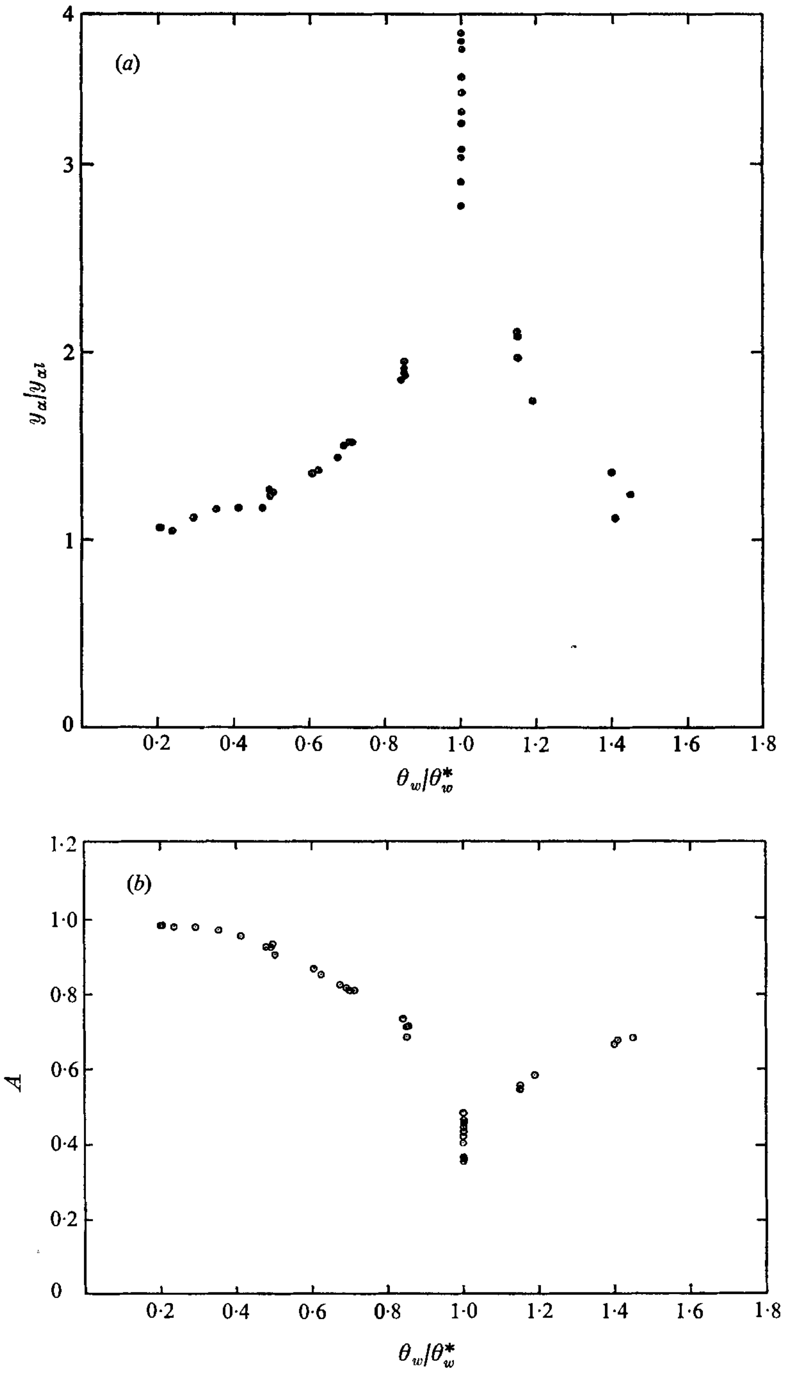

FIGURES 6(*a*) and (*b*). For legend see facing page.

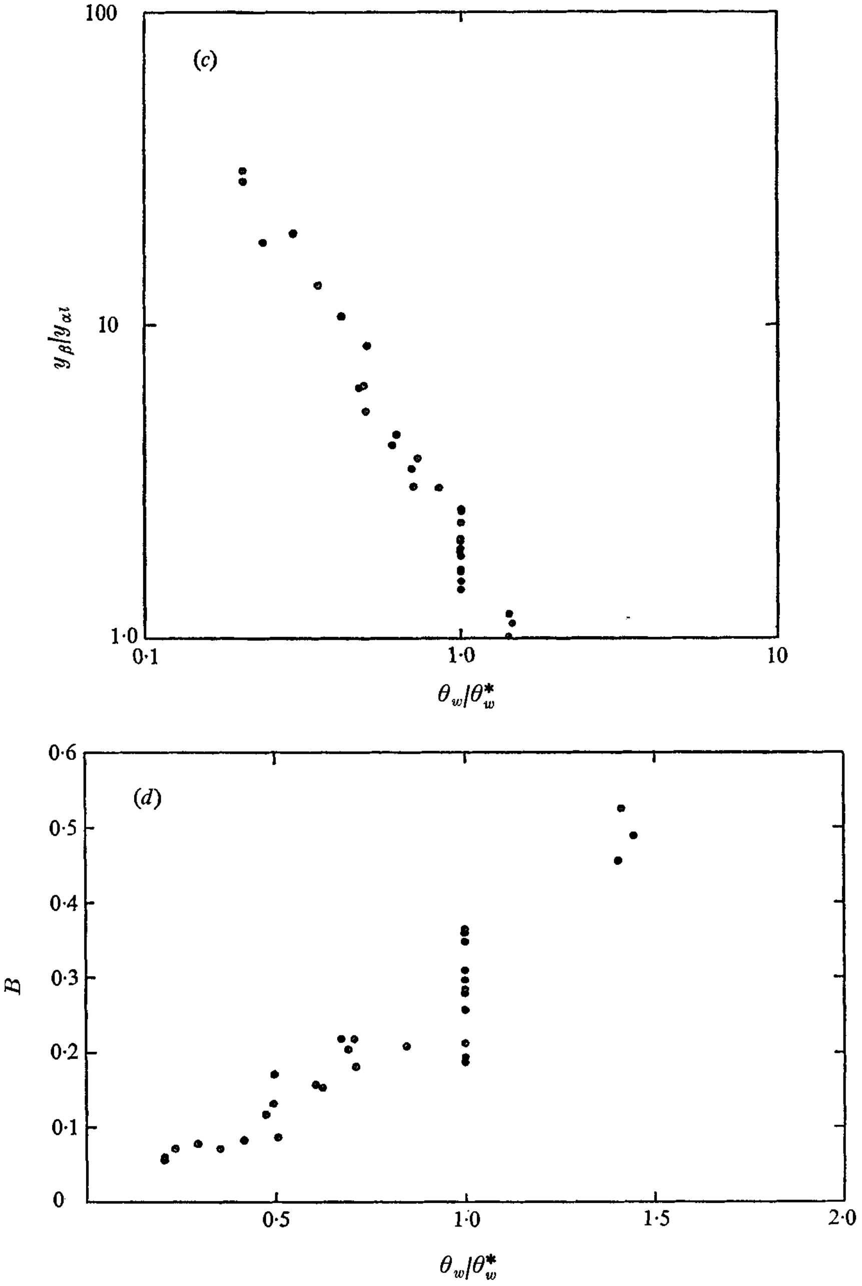

FIGURE 6. Plot of (*a*) $y_\alpha/y_{\alpha l}$, (*b*) A, (*c*) $y_\beta/y_{\alpha l}$ and (*d*) B against θ_w/θ_w^*.

Dain & Hodgson discuss in more detail this analogy between the two types of flow.

4. Entropy production and entropy layer

The real-gas entropy is increased by two mechanisms: the standard frozen shock entropy production and the production due to non-equilibrium relaxation. In flows with strong shocks the frozen shock production is no doubt dominant, but we shall show that in the type of flow discussed here the production due to relaxation is the more important.

On the wedge surface there is an entropy jump across the frozen shock followed by a continuous entropy increase due to relaxation. Through the fully dispersed wave at infinity there is an entropy increase solely due to relaxation, but this increase can also be calculated from the equilibrium shock relations without any knowledge of the non-equilibrium processes. It is of the same order as the increase across the frozen shock at the tip and in fact very slightly smaller. We can make an interesting physical check on the mechanism of entropy production by showing that the integrated entropy production due to the relaxation processes occurring within the shock wave is asymptotically equal to the entropy jump given by the equilibrium shock relations. For the numerical example of § 2 the agreement was excellent.

On the wedge surface the entropy increase across the frozen shock is of order θ_w^3. Along the wedge the entropy increase due to a small change of vibrational energy is

$$ds = (T_{\mathrm{vib}}^{-1} - T^{-1})\,d\sigma, \tag{26}$$

where it has been assumed that the vibrational mode is in internal equilibrium, so that it is possible to define a vibrational temperature T_{vib}. With

$$\bar{\sigma} = \bar{\sigma}_\infty + c_{\mathrm{vib}}(T-1), \quad \sigma = \bar{\sigma}_\infty + c_{\mathrm{vib}}(T_{\mathrm{vib}}-1)$$

the entropy production along the wedge becomes

$$\Delta s = \int_{\bar{\sigma}_\infty}^{\sigma} \frac{c_{\mathrm{vib}}(\bar{\sigma}-\sigma)\,d\sigma}{(c_{\mathrm{vib}}+\bar{\sigma}-\bar{\sigma}_\infty)\,(c_{\mathrm{vib}}+\sigma-\bar{\sigma}_\infty)}. \tag{27}$$

An approximate solution is obtained by using the fact that on the wedge

$$\bar{\sigma}-\sigma = (\bar{\sigma}-\sigma)_0 \exp(-x/x_w), \tag{28}$$

where x_w is the relaxation distance on the wedge surface (measured in the x direction). With the rate equation in the form

$$V\,d\sigma = \rho(\bar{\sigma}-\sigma)\,dx/\cos\theta_w \tag{29}$$

we get

$$\Delta s = c_{\mathrm{vib}} \int_0^x \frac{\rho(\bar{\sigma}-\sigma)^2\,dx}{V\cos\theta_w(c_{\mathrm{vib}}+\bar{\sigma}-\bar{\sigma}_\infty)\,(c_{\mathrm{vib}}+\sigma-\bar{\sigma}_\infty)}. \tag{30}$$

Neglecting terms in the integrand of order θ_w^3 and writing $(\bar{\sigma}-\sigma)_0 = c_{\mathrm{vib}}(T_0-1)$, this becomes

$$\Delta s = c_{\mathrm{vib}}(T_0-1)^2 x_w[1-\exp(-2x/x_w)]/2V_0\cos\theta_w$$

and for $x \to \infty$ $$\Delta s_\infty = c_{\text{vib}}\rho_0(T_0-1)^2 x_w/2V_0 \cos\theta_w. \tag{31}$$

For c_{vib} of order one this is of order θ_w^2 and for small values of θ_w is therefore much larger than the entropy production across the frozen shock at the tip or the equilibrium shock at infinity.

The entropy layer on the wedge has a width of the same order as the development distance and within it there is a gradual transition from an entropy value of order θ_w^2 on the surface to one of order θ_w^3 at infinity.

5. Experiments

The experiments were performed in the Manchester University Mark II shock tube, which has a working section 50 × 200 mm. A wedge model of included angle 7·4°, chord 36 mm and span 200 mm was supported at different incidences in the working section giving possible inclinations of the upper surface to the free stream between 0 and 5°. Choking was prevented by insertion of a plate of thickness 12·7 mm on the floor of the working section upstream of the wedge. This plate extended to the front of the rectangular section, which has the form of a scoop inserted in the first part of the low-pressure circular section of the shock tube of diameter 300 mm. As will be seen from the photographs (figure 7, plate 1), the expansion at the rear end of the plate did not affect the flow on the upper surface of the wedge.

Tests were first made using schlieren observations to check that the flow was steady and uniform, and the main observations were made using interferometry. Typical photographs are shown in figures 7 (*a*) and (*b*). The test gases were carefully dried N_2O (figure 7*a*) and CO_2 (figure 7*b*). These two gases have similar thermodynamic properties but differing relaxation frequencies and large specific heats of vibration at moderate temperatures, the characteristics temperature of the bending modes being 847 °K for N_2O and 959 °K for CO_2.

Figure 7 (*a*) shows a flow of N_2O with a free-stream equilibrium Mach number of 1·68. Using the data of Rees (1968) and Bhangu (1966), the vibrational specific heat, relaxation frequency per unit density, pressure and temperature in the free stream were calculated as $2{\cdot}28R'$, $5{\cdot}3\times10^6\,\text{s}^{-1}\,\text{amagat}^{-1}$, 21·8 kPa and 583 °K.

Figure 7 (*b*) shows a flow of CO_2 with the same free-stream equilibrium Mach number. Using the data of Rees (1968) and Johannesen *et al.* (1962) the vibrational specific heat, relaxation frequency per unit density, pressure and temperature in the free stream were calculated as $2{\cdot}19R'$, $0{\cdot}89\times10^6\,\text{s}^{-1}\,\text{amagat}^{-1}$, 22·4 kPa and 597 °K.

Comparison of figures 7 (*a*) and (*b*) shows the scaling effect of the relaxation frequency. The theoretical density fields were calculated using the methods described in § 2. The fringe shifts are related to the density field by the equation

$$\Delta N(x',y') = (D'K/\lambda\rho_0')(\rho'(x',y')-\rho_\infty'), \tag{32}$$

where D' is the width of the shock-tube working section, K the Gladstone–Dale constant for light of wavelength λ and ρ_0' is the density of the gas at normal

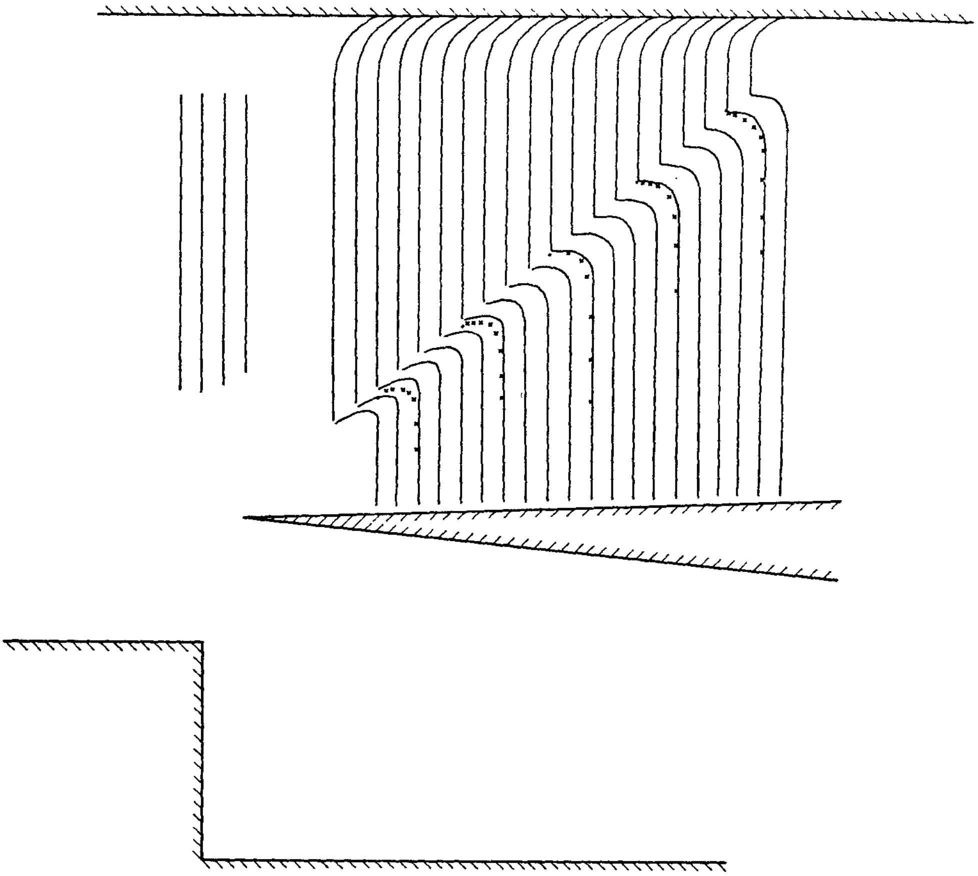

FIGURE 8. Comparison of experimental and theoretical fringe patterns for flow in N_2O with $\theta_w = 2{\cdot}00°$, $M_{e\infty} = 1{\cdot}68$ and $c_{vib} = 2{\cdot}28$. ——, experiment; ×, theory; ●, frozen shock location from theory.

temperature and pressure. With a light source with $\lambda = 4370\,\text{Å}$, $D'K/\lambda$ was 240 for N_2O and 212·1 for CO_2.

The calculated and measured fringe patterns are compared in figure 8 for N_2O and in figure 9 for CO_2. The differences can reasonably be ascribed to the failure of the experiments to model the theoretical flow. Most important are the effects of the small but, nevertheless, finite bluntness of the wedge and the interaction of the shock wave with the side-wall boundary layers. The scales of the relaxation effects do however compare favourably and we feel justified in concluding that the theory gives the more accurate evaluation and that improvements in the experimental techniques, which would in fact be very difficult to achieve, would lead to improved agreement with theory.

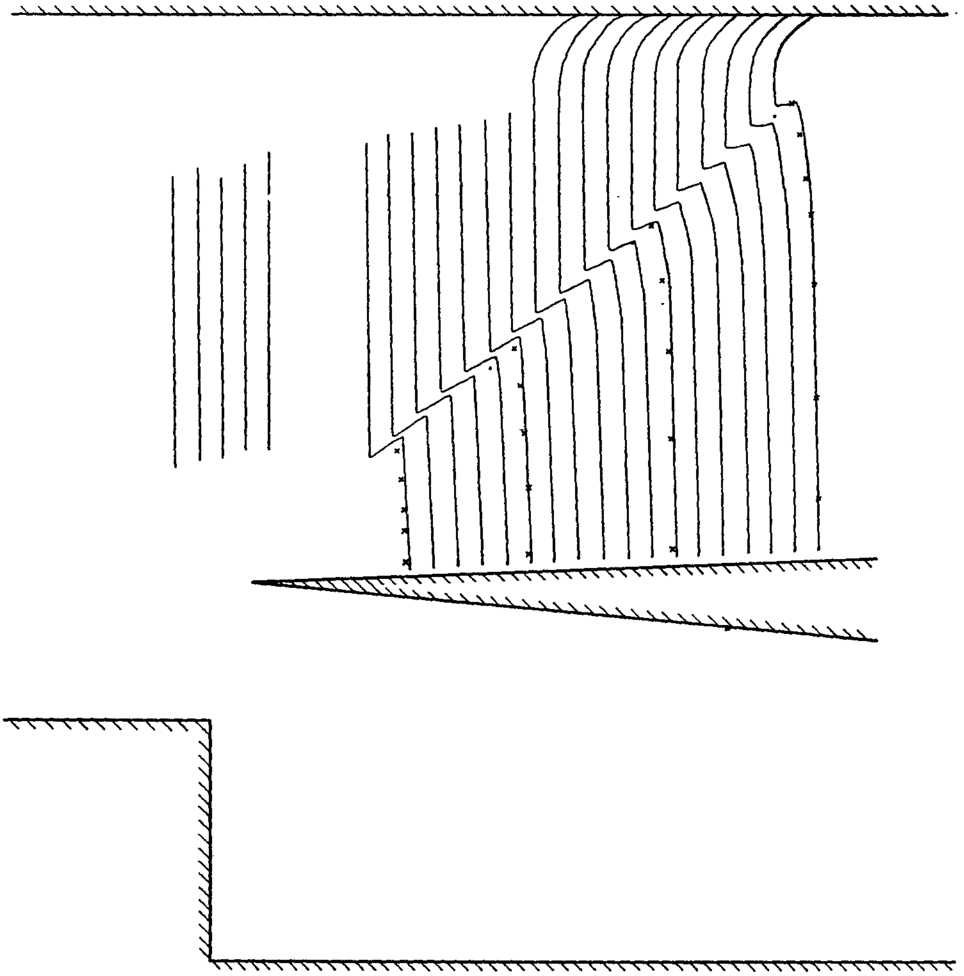

FIGURE 9. Comparison of experimental and theoretical fringe patterns for flow in CO_2 with $\theta_w = 2{\cdot}00°$, $M_{e\infty} = 1{\cdot}68$ and $c_{\mathrm{vib}} = 2{\cdot}19$. ——, experiment; ×, theory; ●, frozen shock location from theory.

6. Conclusions

It has been demonstrated that the initial flow close to the wedge tip can be described by the initial gradients, which are known exactly, and that the far field can be described with sufficient accuracy by four computationally determined universal functions which define the decay of the frozen shock and the far-field development. Dain & Hodgson (1975) present identical conclusions for the flow initiated by an impulsively started piston and draw the appropriate conclusions about the similarity between these two types of flow.

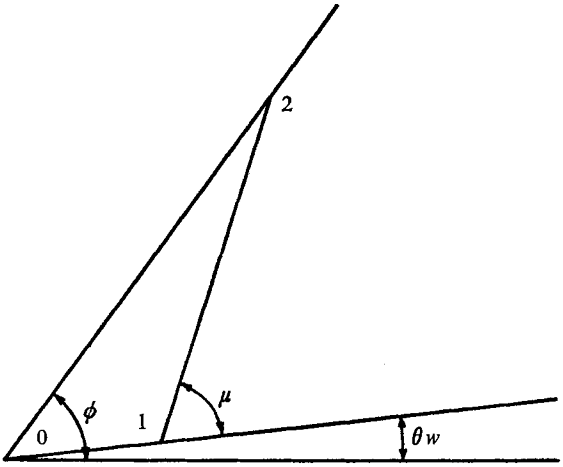

FIGURE 10. Network for calculation of initial gradients.

We have had many valuable discussions with Dr J. P. Hodgson and Dr C. G. Dain. The first author was in receipt of a Research Studentship from the S.R.C. This work has been carried out with support from Procurement Executive, Ministry of Defence.

Appendix

The tip gradients have been derived by several authors, e.g. Capiaux & Washington (1963) and Sedney (1970). To translate their results into our notation is a lengthy process and we therefore present a simple derivation directly from the compatibility relations for a left-hand characteristic 1–2 in figure 10. We also indicate briefly how the particular gradients relevant to our investigation can be derived. In particular, we present a simple derivation of the linear value for the frozen shock decay distance.

The compatibility relation for the characteristic 1–2 is, from (11),

$$\frac{p_2-p_1}{\rho_0 V_0^2 \tan\mu_0}+\theta_2-\theta_w=-\frac{(\gamma-1)\rho_0\Gamma_0(y_2-y_1)}{V_0^3\sin\mu_0\sin(\theta+\mu)_0}. \tag{A 1}$$

From the geometry of figure 10 we have

$$y_2-y_1=\frac{\sin(\theta+\mu)_0\sin(\phi-\theta)_0}{\sin\mu_0}dz, \tag{A 2}$$

and making use of the component of the momentum equation perpendicular to the wedge surface, which gives that to the first order the normal pressure gradients are zero, we have

$$p_2-p_1=\frac{\tan(\phi-\theta)_0}{\tan\mu_0}dp, \tag{A 3}$$

where dp is the pressure change along the frozen shock wave behind the shock.

Hence

$$\left(\frac{dp}{dz}\right)_0 = -\frac{(\gamma-1)\,\rho_0^2\,\Gamma_0\cos(\phi-\theta)_0}{V_0[\cos^2\mu_0+\rho_0\,V_0^2\cot(\phi-\theta)_0\sin^2\mu_0(d\theta/dp)_0]}, \tag{A 4}$$

where $(d\theta/dp)_0$ is taken along the shock wave and is known from the standard relations for oblique shock waves.

The pressure gradient along the wedge is

$$\left(\frac{dp}{dl}\right)_0 = \left(\frac{dp}{dz}\right)_0\Big/\cos(\phi-\theta)_0. \tag{A 5}$$

From these gradients it is easy to find any other gradient which may be required. In particular, we can find the gradient of the departure from equilibrium used in plotting the decay of the frozen shock.

The curvature of the frozen shock at the tip is

$$k_{s0} = \left(\frac{dp}{dz}\right)_0\Big/\left(\frac{dp}{d\phi}\right)_0. \tag{A 6}$$

The energy equation may be written as

$$(c_p/c_{\text{vib}})\,d\bar{\sigma}+d\sigma+V\,dV = 0. \tag{A 7}$$

Along the frozen shock $d\sigma = 0$ and since

$$\partial/\partial z = k_s\,\partial/\partial\phi, \quad dz = dy/\sin\phi$$

we have

$$\frac{c_p}{c_{\text{vib}}}\left(\frac{d(\bar{\sigma}-\sigma)}{dy}\right)_0 = -\frac{V_0(dp/dz)_0\,(dV/d\phi)_0}{\sin\phi_0(dp/d\phi)_0}, \tag{A 8}$$

so that

$$\left[\frac{d\log\Gamma_\alpha/\Gamma_0}{dy}\right] = -y_{\alpha_0}^{-1} = \frac{c_{\text{vib}}/c_p(\gamma-1)\,\rho_0^2\cos(\phi-\theta)_0(dV/dp)_0}{[\cos^2\mu_0+\rho_0\,V_0^2\cot(\phi-\theta)_0\sin^2\mu_0(d\theta/dp)_0]\sin\phi_0}, \tag{A 9}$$

where $(dV/dp)_0$ is known from the oblique shock wave relations.

In the linear approximation

$$V\,dV = -dp/\rho, \tag{A 10}$$

$$dV/dp = -1/\gamma^{\frac{1}{2}}M_\infty, \tag{A 11}$$

$$d\theta/dp = (M_\infty^2-1)^{\frac{1}{2}}/\gamma M_\infty^2, \tag{A 12}$$

so that

$$\left[\frac{d\log\Gamma_\alpha/\Gamma_0}{dy}\right]_0 = -y_{\alpha l}^{-1} = \frac{c_{\text{vib}}(\gamma-1)\,M_\infty}{2c_p\gamma^{\frac{1}{2}}(M_\infty^2-1)^{\frac{1}{2}}}. \tag{A 13}$$

It is slightly more difficult to find

$$-y_{\beta_0}^{-1} = \left[d\log\left(\frac{\Gamma_{\max}-\Gamma_{\max\infty}}{\Gamma_0-\Gamma_{\max\infty}}\right)\Big/dy\right]_0.$$

Γ_0 is known but $\Gamma_{\max\infty}$ will have to be found in each case by first determining the wave angle at infinity either by trial and error or by solving the shock wave cubic. This gives the normal Mach number at infinity, and the equilibrium shock wave structure can then be determined. The analytical expressions will not be given here. In our calculations $\Gamma_{\max\infty}$ was found directly during the computational procedure.

REFERENCES

BHANGU, J. K. 1966 Shock tube studies of vibrational relaxation in N_2O. *J. Fluid Mech.* **25**, 817.

BLYTHE, P. A. 1969 Non-linear wave propagation in a relaxing gas. *J. Fluid Mech.* **37**, 31.

CAPIAUX, R. & WASHINGTON, M. 1963 Non-equilibrium flow past a wedge. *A.I.A.A. J.* **1**, 650.

DAIN, C. G. & HODGSON, J. P. 1975 The development of weak waves in the unsteady one-dimensional flow of a vibrationally relaxing gas ahead of an impulsively started piston. *J. Fluid Mech.* **69**, 129.

DER, J. J. 1963 Theoretical studies of supersonic two-dimensional and axisymmetric non-equilibrium flow including calculations of flow through a nozzle. *N.A.S.A. Tech. Rep.* R-164.

HODGSON, J. P. & JOHANNESEN, N. H. 1971 Real-gas effects in very weak shock waves and the structure of sonic bangs. *J. Fluid Mech.* **50**, 17.

JOHANNESEN, N. H., ZIENKIEWICZ, H. K., BLYTHE, P. A. & GERRARD, J. H. 1962 Experimental and theoretical analysis of vibrational relaxation regions in CO_2. *J. Fluid Mech.* **13**, 213.

LIGHTHILL, M. J. 1956 Viscosity effects in sound waves of finite amplitude. In *Surveys in Mechanics* (ed. Batchelor & Davies), pp. 250–351. Cambridge University Press.

REES, T. 1968 Computer calculations of relaxation regions and equilibrium conditions for shock waves with tables for CO_2 and N_2O. *Aero. Res. Counc. R. & M.* no. 3472.

SEDNEY, R. 1970 The method of characteristics. In *Non-equilibrium Flows* (ed. Wegener), part 2, pp. 160–225. Dekker.

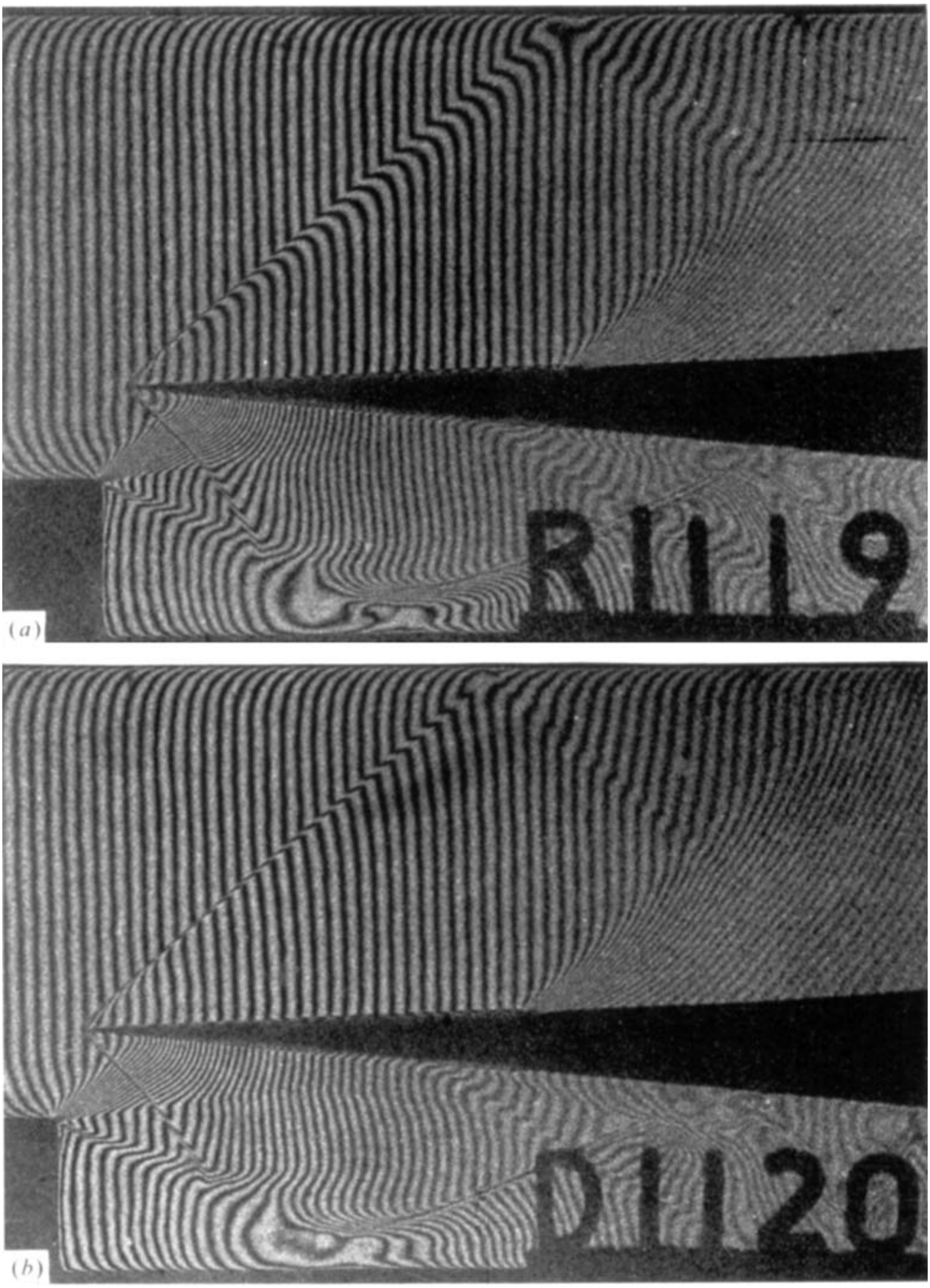

FIGURE 7. Flows of (*a*) N_2O and (*b*) CO_2 with a free-stream equilibrium Mach number of 1·68.